Comparison of Spacecraft Charging Environments at the Earth, Jupiter, and Saturn

Henry B. Garrett and Alan R. Hoffman

***Abstract*—Studies of the Earth with the ATS-5, ATS-6, and SCATHA spacecraft led to the development of several simple tools for predicting the potentials to be expected on a spacecraft in the space environment. These tools have been used to estimate the expected levels of worst case charging at Jupiter and Saturn for the Galileo and the Cassini spacecraft missions. This paper reviews those results and puts them in the context of the design issues addressed by each mission including the spacecraft design mitigation strategies adopted to limit differential charging. The model shows that shadowed surfaces in Earth orbit can reach ∼25 kV or higher in worst case environments. For Galileo, spacecraft-to-space potentials of ∼900 V were predicted in shadow. Since such potentials could produce possible discharges and could effect low energy plasma measurements, the outer surface of Galileo was designed to rigid conductivity requirements. Even though the surface of Galileo is not entirely conducting, after 27 orbits no adverse effects due to surface charging aside from limited effects on low energy plasma measurements have been reported. The saturnian environment results in spacecraft potentials to space in shadow of ∼100 V or less. Although the overall surface of the Cassini spacecraft was not entirely conducting and grounded, it is shown that only in the most extreme conditions, is it expected that Cassini will experience any effects of surface charging at Saturn.**

***Index Terms*—Plasma environments, space weather, spacecraft charging.**

I. Introduction

ONE of the best known space plasma interactions at the Earth is surface charging at geosynchronous orbit. Surface charging is not just a concern for spacecraft in geosynchronous orbit [1], however, but also to a varying degree in other regions of the Earth's magnetosphere and throughout the solar system. In particular, high levels of charging (greater than a few hundred volts) are expected in the Earth's auroral zones at high latitudes [2] and at Jupiter [3], [4]. (Note: in general, high surface potentials are not of concern to spacecraft systems, rather it is the differential potentials between adjacent surfaces that are of concern as they can lead to arcing—indeed, potential differences as low as ∼100 V are believed capable of inducing arcing. See [5] for a thorough discussion of surface charging, its estimation, and various mitigation techniques.) Here a simple software tool developed for the Earth's environment is extended to predict surface potentials at Jupiter and Saturn. This tool and it results have been described in great detail in the open literature [6], [7]. The tool was used by the Galileo and Cassini missions in determining the maximum and minimum charging potentials expected (and thus presumably the worst case differential potential possible) and hence the design requirements for surface potential mitigation. In this paper, the Earth's, Jupiter's, and Saturn's charging environments are described. The basic assumptions of the simple tool used for calculating charging will then be reviewed and the estimated nominal range of surface potentials for each of the environments presented. The estimated nominal charging levels for Earth and, at least preliminarily, Jupiter and Saturn are consistent with observations demonstrating to first order the value of the tool for mission design. Finally, the assumptions of the model will be varied to test the range of possible worst case conditions.

Manuscript received November 1, 1999; revised May 1, 2000. The research in this paper was carried out by the Jet Propulsion Laboratory, California Institute of Technology under contract with the NASA.

The authors are with with the Safety and Mission Assurance Directorate, Jet Propulsion Laboratory, California Institute of Technology, Pasadena, CA 91109 USA.

Publisher Item Identifier S 0093-3813(00)10650-2.

II. The Environments

Table I lists the principal characteristics of the terrestrial, jovian, and saturnian magnetospheres. As shown in this table, Jupiter and Saturn are roughly ten times the size of the Earth while their magnetic moments are, respectively, 10^5 and 10^3 larger. As the magnetic field at the equator is proportional to the magnetic moment divided by the cube of the radial distance, the terrestrial and saturnian magnetospheres scale similarly relative to their planetary radii. The jovian magnetic field, however, is 100 times larger. An additional consideration is that the photoelectron flux at 1 AU (corresponding to approximately 2.0 nA/cm^2 for an aluminum surface) for the Earth is ∼25 times that at Jupiter (∼5 AU) and ∼100 times that at Saturn (∼10 AU).

The rotation rate is also an important factor. Both Jupiter and Saturn spin over twice as fast as the Earth–∼10 h versus 24 h. Given their strong magnetic fields, this means that the cold plasma trapped in these magnetospheres is forced to co-rotate at velocities much higher than a spacecraft's orbital velocity. This is opposite to the situation at Earth where, at low altitudes, a spacecraft orbits at ∼8 km/s faster than the ionospheric plasma. Co-rotation velocities can range from 30–40 km/s near Jupiter and Saturn to over 100 km/s in their outer magnetospheres. In particular, at Jupiter strict co-rotation breaks down at approximately 20 R_j (∼200 km/s) [4] whereas at Saturn this occurs at about 10 R_s (∼100 km/s) [8]. Closely related to the co-rotation velocity is the *in situ* cold plasma density variation. At the Earth, the only source is the ionosphere so that the cold plasma population falls to a few particles per cubic centimeter by 4–5 R_e. At Jupiter, the moon Io at 5.9 R_j is an additional source of cold plasma that then extends well out into the magnetosphere (∼20 R_j or farther). At Saturn, in addition to its rings, there is an additional source of cold plasma from the moon Titan at ∼20 R_s.

0093–3813/00$10.00 © 2000 IEEE

TABLE I
THE PLANETS' MAGNETOSPHERES

Earth	
-equatorial radius (km)	6.38×10^3
-magnetic moment (G-cm^3)	8.10×10^{25}
-rotation period (hrs)	24.0
-aphelion/perihelion (au)	1.01/0.98
Jupiter	
-equatorial radius (km)	7.14×10^4
-magnetic moment (G-cm^3)	1.59×10^{30}
-rotation period (hrs)	10.0
-aphelion/perihelion (au)	5.45/4.95
Saturn	
-equatorial radius (km)	6.00×10^4
-magnetic moment (G-cm^3)	4.30×10^{28}
-rotation period (hrs)	10.23
-aphelion/perihelion (au)	10.06/9.01

These cold ion populations tend to suppress surface charging on the side of the vehicle that they impact.

As the magnetosphere is the primary controlling factor for the local plasma environments, the charging environment differs for each of these planets. Representative values for the primary plasma environments at the Earth, Jupiter, and Saturn are presented in Table II. The differences evident in this table and their consequences will be described in the following paragraphs.

A. Earth

The Earth has one of the most complex and variable magnetospheres in the solar system. As will be shown, it may also have the highest charging levels. In terms of a simple schematic of the Earth's magnetosphere, there are four main plasma populations. Starting with the lowest latitude regime, the "ionospheric" population extends the cold ionosphere out along closed field lines to 3 to 5 R_e (typically called the plasmasphere). The plasma varies from a density of $\sim 10^6$ cm^{-3} (O^+ dominated) at 100 km to $\sim$100 cm^{-3} (H^+) at 4 to 5 R_e. The mean energy varies from a few tenths of an electronvolt at low altitudes to 10–100 eV at high altitude. The auroral regime is at higher latitudes and extends out to higher altitudes. This population is represented by the aurora at low altitudes and the plasmasheet at geosynchronous orbit. The plasma typically consists of an electron/H^+ composition with several tens of kiloelectronvolt mean energy and densities of 0.1–2 cm^{-3}. Superimposed on these two regimes is the Van Allen regime marked by the trapped radiation belts. These consist primarily of high energy ($E > 100$ keV) electrons and protons. Although of small direct importance to surface charging at the Earth, the high energy electrons are the primary source of internal charging. The final regime, the very high latitude regime, is characterized by low densities (0.1 cm^{-3}) and energies (200 eV) with occasional bursts of high velocity streams (800 km/s). The field lines at very high latitudes eventually couple with the interplanetary magnetic field.

B. Jupiter

The magnetosphere of Jupiter is dominated by three factors: the magnetic field tilt (11°) relative to its spin axis, its rapid rotation, and the jovian moon Io at 5.9 R_j. Io generates a vast torus of gas and ions. The more rapid rotation of Jupiter's magnetic field forces the cold plasma associated with this torus to accelerate and expand by centrifugal force into a giant disc. The magnetic field tilt and rotation rate cause the plasma disc to wave up and down so that at a given location plasma parameters vary radically during a 10 h period. Jupiter's environment can be roughly divided into three populations: the cold plasma associated with the Io torus and the plasma disc ($0 < E < 1$ keV), the intermediate plasma (1 keV $< E < 60$ keV), and the radiation environment ($E > 60$ keV). The cold plasma is characterized by high densities ($\sim$2000 cm^{-3}) and low energies. The plasma consists of hydrogen, oxygen (singly and doubly ionized), sulfur (singly, doubly, and triply ionized), and sodium (singly ionized) ions. Intermediate energy electrons ($\sim$1 keV) and protons ($\sim$30 keV) at Jupiter are assumed to vary exponentially from $\sim$5 cm^{-3} for $r < 10R_j$ to 0.001 cm^{-3} beyond 40 R_j [4]. Co-rotation velocities vary from $\sim$45 km/s at 4 R_j to $\sim$200 km/s at 20 R_j.

C. Saturn

Saturn is marked by a magnificent set of rings that are its most obvious feature and set it apart from all the other planets. Aside from the rings, however, Saturn's magnetosphere resembles Jupiter's—a cold inner plasma disk that becomes a lower density, slightly higher energy plasma disk at large distances. Although there is no "Io-equivalent" moon in the inner magnetosphere, there is a fairly dense cold plasma sheet. At $\sim$20 R_s, Saturn's huge moon Titan contributes a large cloud of neutral gas in the outer magnetosphere. Unlike Jupiter, Saturn's magnetic field axis is apparently aligned with the spin axis so that the plasma ring around Saturn is relatively steady compared to that of Jupiter. Plasma co-rotation velocities are similar to Jupiter although maximum velocities tend to peak at $\sim$100 km/s with co-rotation breaking down at $\sim$10 R_s.

III. THE MAJOR CURRENT TERMS

A mathematical model capable of first-order estimates of spacecraft surface to space plasma potential (charging potential) for a variety of conditions has been developed [6] and reviewed in detail in the open literature [7]). The model (or design tool) is based on current balance. Incoming electrons and ions are balanced by photoemission, backscattering, and secondary

TABLE II
REPRESENTATIVE VALUES OF THE CHARGING ENVIRONMENT AT THE EARTH, JUPITER, AND SATURN. THE HEADINGS ARE DESCRIBED IN THE TEXT

Region	Jph	re1	te1	re2	te2	rek	tek	ak	rhk	thk	hk	Vc	rhc	thc	Am	roc	toc	eV(H)	eV(Am)
Earth																			
ionosphere	2.00	100000	0.2	-	-	-	-	-	-	-	-	8	-	-	16	100000	0.1	-	5.38
plasmasphere	2.00	1000	0.2	-	-	-	-	-	-	-	-	8	-	-	16	1000	1	-	5.38
auroral zone	2.00	5000	0.2	1.12	12000	-	-	-	-	-	-	8	-	-	16	5000	0.1	-	5.38
geosynchronous	2.00	-	-	1.12	12000	-	-	-	-	-	-	3	0.24	29500	16	-	-	-	0.76
Jupiter																			
cold torus 3.5 Rj	0.08	50	0.5	-	-	5	1000	2.1	1	30000	2.0	44	-	-	32	50	0.5	10	325
warm torus 5.5 Rj	0.08	1000	1	-	-	10	1000	2.0	1	30000	3.0	69	-	-	24	1000	2	25	600
hot torus 7 Rj	0.08	1000	10	-	-	5	500	2.0	5	50000	4.2	85	-	-	24	1000	40	38	911
plasmasheet 8 Rj	0.08	12	50	-	-	2	500	2.0	5	40000	3.5	100	-	-	16	12	50	53	840
outer mag 20 Rj	0.08	-	-	-	-	0.01	1000	2.0	-	-	-	250	0.01	1000	1	-	-	328	328
Saturn																			
inner plasma- sheet 4-8 Rs	0.02	2.15	20	-	-	0.196	262	1.8	0.005	29833	7.4	40	3.20	14	16	30.15	73	8	134
extended plasma-sheet 8-12 Rs	0.02	0.72	28	-	-	0.111	458	1.7	0.003	30800	8.5	80	0.74	26	16	2.50	246	34	538
outer mag 12-20 Rs	0.02	0.10	41	-	-	0.037	583	2.6	0.001	18800	6.7	100	0.24	37	16	0.54	420	53	840

emission. The program varies the spacecraft-to-space potential until the total current is zero according to the following equation:

$$I_T(V) = (I_I(V) + I_{\rm SE}(V) + I_{\rm SI}(V) + I_{\rm BSE}(V) + I_{\rm PH}(V)) - I_E(V) \quad (1)$$

where

V surface potential relative to space;
I_T total current to spacecraft surface at V; 0 at equilibrium when all the current sources balance;
I_E incident electron current;
I_I incident positive ion current;
$I_{\rm SE}$ secondary emitted electron current due to I_E;
$I_{\rm SI}$ secondary emitted electron current due to I_I;
$I_{\rm BSE}$ backscattered electron current due to I_E;
$I_{\rm PH}$ photoelectron current.

The incident electron and ion currents are typically estimated by integrating the appropriate Maxwellian distributions (3) to obtain the current as a function of temperature, number density, and potential for a "thick sheath" spherical probe:

$$I_E = \begin{cases} I_{E0}\exp(qV/E_E) & V < 0 \\ I_{E0}(1+qV/E_E) & V > 0 \end{cases}$$
$$I_I = \begin{cases} I_{I0}\exp(-qV/E_I) & V > 0 \\ I_{I0}(1-qV/E_I) & V < 0 \end{cases} \quad (2)$$

where

I_{E0} ambient electron current;
I_{I0} ambient positive ion current;
E_E characteristic energy of electrons;
E_I characteristic energy of ions;
q charge.

The secondary and backscatter surface currents are then obtained by integration over the incident currents; the results have been parameterized by fitting them in terms of the temperature, number density, and potential (see [6] and [7] for a thorough discussion of each function). The charging properties of aluminum are used in this study because aluminum is representative of a common spacecraft surface material and typically represents a worst case. The photoelectron current is similarly parameterized in terms of the potential and material.

The basic Maxwellian distribution is given by

$$F_M = N(M/2\pi E_o)^{3/2} e^{-E/E_o} \quad (3)$$

where

M particle mass;
F_M Maxwell–Boltzmann distribution;
N number density;
E_o characteristic energy of plasma;
E particle energy.

Whereas Maxwellian distributions adequately represent many of the plasma environments encountered in space, they are often inadequate for explaining the complex environments at Jupiter and Saturn. For co-rotating ion plasmas, a "ram" approximation is often more appropriate for the ion current

$$I_R = \pi R^2 N V_S \quad (4)$$

where

I_R "Ram" current;
R radius of spherical spacecraft;
V_S spacecraft velocity relative to plasma.

The Jovian and Saturnian environments are characterized by a harsher radiation environment at high energies than the Earth's. As a result, a Maxwellian distribution does not join smoothly onto the high energy spectra for the protons and electrons. If the latter power law spectra are cut off at an arbitrary low energy, the resulting discontinuity causes difficulties in computing the total current density of the electrons to a satellite surface in the jovian and saturnian environments.

To derive a smooth distribution function for the warm electrons and protons, the Kappa distribution function [9] F_κ in cm^{-6} s^3 was employed

$$F_\kappa = N(M/2\pi E_o)^{3/2}\kappa^{-3/2} \cdot \frac{\Gamma(\kappa+1)}{\Gamma(\kappa-1/2)\,(1+E/\kappa E_o)^{\kappa+1}} \quad (5)$$

where

F_κ Kappa distribution;
Γ Gamma function;
κ Kappa factor (constant).

As κ goes to infinity, (5) becomes a Maxwellian distribution. As E goes to infinity, the form of the distribution approaches

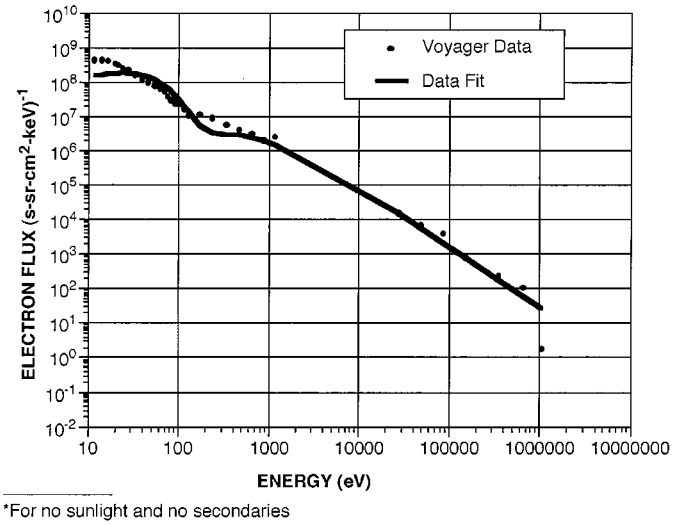

Fig. 1. Maxwellian (below 1 keV) and Kappa (above 1 keV) distribution fits to Voyager 2 inbound electron measurements for Saturn ($L = 11.59$). The potential was estimated to be -480 V in the absence of sunlight and secondary emission for this environment.

a power law. A simple fitting procedure was utilized to determine the values for N, E_o, and κ. First, the omnidirectional high energy fluxes were computed and converted to values of the distribution function at two energies for electrons (36 and 360 keV) and for protons (0.6 and 6 MeV). The warm electron and proton Maxwellian density and temperature were used to determine values of the distribution function at zero energy. Kappa distribution functions were then fit to these values and the high energy flux values. A representative fit for Saturn is presented in Fig. 1. The resulting Kappa distributions were then integrated to give appropriate surface currents as functions of temperature, κ, number density, and potential. For reference, the ratio of the current derived from a Kappa distribution to that of a Maxwellian is

$$\frac{I_{\kappa o}}{I_{Mo}} = \left(\frac{N_\kappa}{N_M}\right)\left(\frac{E_\kappa}{E_M}\right)^{1/2}\left[\frac{\kappa^{1/2}\Gamma(\kappa-1)}{\Gamma(\kappa-1/2)}\right] \tag{6}$$

where

$I_{\kappa o}$ ambient current for Kappa distribution;
I_{Mo} ambient current for Maxwellian distribution;
N_κ ambient density for Kappa distribution;
N_M ambient density for Maxwellian distribution;
E_κ characteristic energy for Kappa distribution;
E_M characteristic energy for Maxwellian distribution.

The current for the repelled and attracted species for a Kappa distribution in the thick sheath approximation are given by

$$I_\kappa = \begin{cases} I_{\kappa o}\left(1+\dfrac{|qV|}{\kappa E_\kappa}\right)^{-(\kappa-1)} & \text{repelled} \\ I_{\kappa o}\left(1+\left(\dfrac{\kappa-1}{\kappa}\right)\dfrac{|qV|}{E_\kappa}\right) & \text{attracted.} \end{cases} \tag{7}$$

Again, as κ goes to infinity, (7) reduce to the appropriate equations for repulsion and attraction for a Maxwellian distribution.

To account for all the currents present at Jupiter and Saturn, (1) was expanded to include a two component electron Maxwellian plasma, a high energy electron Kappa distribution, a high energy proton Kappa component, a cold/co-rotating proton component, a co-rotating heavy ion component, and a Maxwellian proton component. Corresponding secondary and backscatter components were included for each population along with the photoelectron current. Values of these components for the various plasma regions are listed in Table II where

$J_{\rm ph}$ photoelectron current (nA/cm^{-2});
r_{e1} electron cold component density (cm^{-3});
t_{e1} electron cold component characteristic energy (eV);
r_{e2} electron hot component density (cm^{-3});
t_{e2} electron hot component characteristic energy (eV);
r_{ek} electron Kappa component density (cm^{-3});
t_{ek} electron Kappa component characteristic energy (eV);
a_k electron Kappa value;
r_{hk} proton Kappa component density (cm^{-3});
t_{hk} proton Kappa component characteristic energy (eV);
h_k proton Kappa value;
V_c co-rotation velocity (km/s);
r_{hc} proton Maxwellian component density (cm^{-3});
t_{hc} proton Maxwellian characteristic energy (eV);
A_m atomic nucleon number (e.g., He is 4);
r_{oc} heavy ion density;
t_{oc} heavy ion Maxwellian characteristic energy (eV).

Also listed in Table II are the estimated equivalent "thermal" energies of the proton or heavy ion component due to co-rotation. These numbers will be utilized in determining when the co-rotation current component should be used or when the Maxwellian thick sheath current is more appropriate.

IV. Estimated Charging Levels

A. Earth

Given a model of the ambient electron and ion environments in terms of Maxwellian and Kappa distributions and the density and co-rotation velocity of the cold ions, the surface potential for a spacecraft surface can be estimated using the simple spacecraft-to-space thick sheath model described above. Evans *et al.* [10] used the model discussed here to calculate the potentials throughout the terrestrial magnetosphere for a small aluminum sphere in the Earth's shadow. Their results are presented in Fig. 2. This figure is intended to be used as a simple mission planning tool for identifying regions with high charging levels; if a spacecraft were to pass through or near a region of high charge, then appropriate mitigation methods should be considered in the design. The figure identifies basically four regions: the inner plasmasphere with little charging, the geosynchronous orbit (high charging) and its extension into the auroral zone (moderate charging), and the high latitude region (zero charging) giving way to a solar wind environment at large tailward distances (-100 V, the highest value predicted for the solar wind). Examples of the ionospheric, plasmaspheric, auroral, and geosynchronous orbit plasma environment distributions are presented later.

B. Jupiter

Given the high surface potentials found in the Earth's magnetosphere, it was anticipated that Jupiter might also have high potentials (e.g., [3]). Unlike the Earth, however, over a large

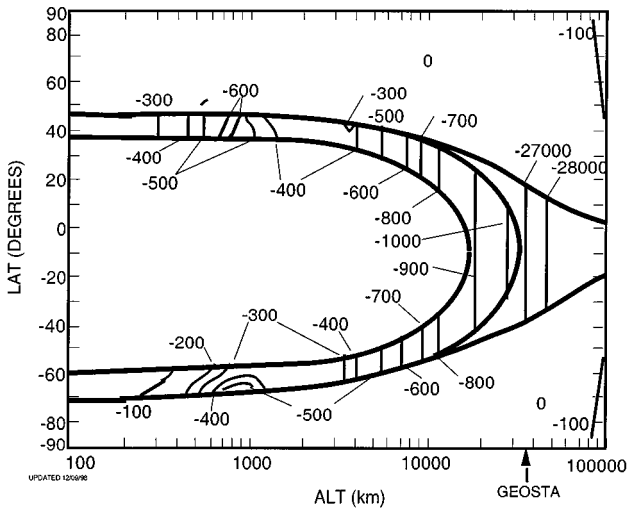

Fig. 2. Surface potential contours (in the absence of sunlight) in volts as a function of altitude and latitude for the Earth [10]. Outside the "horseshoe" region charging is negligible.

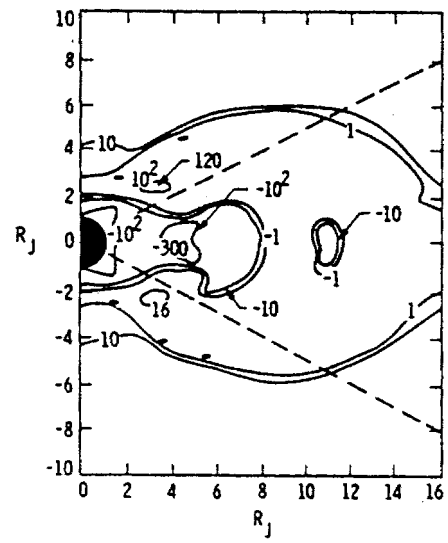

Fig. 3. Spacecraft charging potential contours in volts for the thick sheath approximation in the 110°W sunlit meridian at Jupiter [4]. The horizontal axis represents distance along the rotational equator. Photoelectron and secondary electron currents are included. The dashed lines bracket the region of applicability (observations).

portion of the jovian and saturnian magnetospheres warm energetic electron fluxes are the dominant current source, balancing principally with the photoelectrons. It has proven necessary to represent the 1 to 100 keV electron energy range by a Kappa distribution [4]. In Figs. 3 and 4 [4], the spacecraft-to-space potentials for the jovian magnetosphere have been estimated using the design tool modified to include Kappa distributions and the co-rotating plasma. The potential contours represent the spacecraft-to-space potentials that would be seen for a conducting aluminum sphere in the sunlight (Fig. 3) for a nominal environment and for a worst case environment where both sunlight and secondary emission were suppressed.

The estimates in Fig. 3 for a nominal charging environment are in good agreement (factor of $\sim$2) with those reported for Voyager [11]. This latter paper observed voltages of several tens of volts negative and implied that on one occasion a potential of at least -130 V might have been observed. Likewise, Scudder *et al.* [12] reported potentials of a few tens of volts positive to tens of volts negative in the torus.

It should not be assumed from Fig. 3 that spacecraft charging is not a problem in the jovian environment. Under restrictive conditions, secondary emissions can be suppressed over a small surface. Also, because the sunlight is a factor of 25 less than at the Earth it becomes easier for the ambient electron current to dominate and charge the spacecraft. If the surface is electrically isolated from the vehicle with secondary electron suppression and in the shade so that the photoelectron flux is zero, significant charging can occur as evidenced in Fig. 4. It should be emphasized that this corresponds to an almost pathological case and is presented solely as a means for estimating a worst case for design purposes. A possible example would be a small insulated cavity for a sensor in which one side was illuminated by sunlight creating a space charge over the entrance (suppressing secondary emission from the shadowed interior). In support of such high potential predictions, the Voyagers may have observed tens of kilovolts surface potentials at Jupiter [13]. However, as the

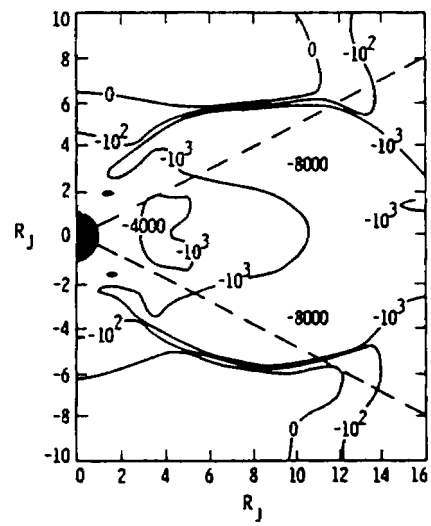

Fig. 4. Spacecraft to space potential contours for the thick sheath approximation [4] as in Fig. 3. No photoelectron or secondary currents are included.

Voyager and Galileo spacecraft were designed so as to mitigate differential surface charging—they were conductive over most of their surfaces and approached the ideal of a conducting sphere–surface arcing has not been observed in flight. However, significant internal charging/discharging may have occurred on Voyager 1 [14].

Based on these charging concerns, the Galileo design was evaluated in detail using the NASCAP code [15], [16] by N. J. Stevens and the design altered to minimize differential potentials as much as possible. In particular, isolated conductors were limited to less than 3 cm^2, cavities were avoided wherever possible, circuits were filtered for electrostatic pulses (particularly near areas where charging might occur), and careful grounding

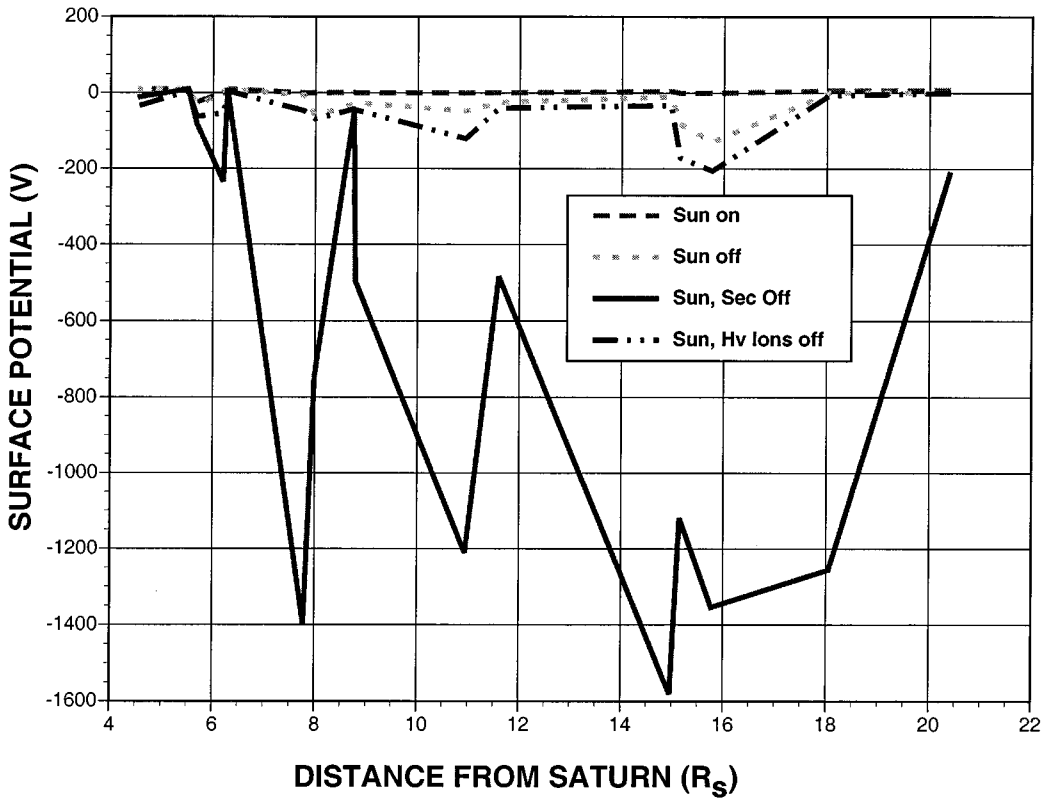

Fig. 5. Spacecraft to space potentials for Saturn as a function of radial distance from the planet for 16 Voyager 1 and 2 spectra for several charging assumptions: sunlit with secondary emission (nominal), shadowed and secondary emission (nominal), and two worst case assumptions: no sunlight, no secondary emissions or no sunlight and no cold, heavy ion current. The potentials are taken from Table III for the "best" expected values.

procedures were followed throughout the design and construction process. After more than four years in orbit at Jupiter, no problems have been attributed to electrostatic surface discharge on the Galileo spacecraft.

C. Saturn

The charging environment at Saturn resembles that at Jupiter. As a comprehensive plasma model such as those developed for Jupiter and the Earth has not been completed for Saturn, contour plots like those in Figs. 2–4 are not available. Instead, a set of 16 electron and ion spectra covering the L-shell range from $\sim$4 to $\sim$21 was reconstructed from the Voyager 1 and 2 flybys [8], [17], [18] for the purpose of estimating the expected potentials. A representative electron spectrum is presented in Fig. 1. Each set of electron spectra was fit by a Maxwellian at low energies ($\sim$10 to 1000 eV) and by a Kappa distribution from 1 to 100 keV. The cold plasma populations (hydrogen and oxygen ions) were fit by either a Maxwellian or co-rotation velocity. The proton population above 1 keV was fit by a Kappa distribution. The 16 saturnian spectra used in this analysis are tabulated in the Appendix. Note that the "second Maxwellian" component is only listed for completeness—it was used in deriving the Kappa distributions for the electrons and for testing purposes, not for the potential derivations. The co-rotating velocity was assumed to vary with distance up to about $10R_s$ and be $\sim$100 km/s over the rest of the range studied ($\sim$10 to $\sim$20 R_s). This is based on [8].

Fig. 5 and Table III give the potentials calculated by the tool for the 16 spectra for several charging assumptions: sunlit with secondary emission (nominal), shadowed and secondary emission (nominal), and two worst case assumptions: no sunlight, no secondary emissions or no sunlight and no cold, heavy ion current. Table III calculates the potentials for two different current collection assumptions: ram (mode 2) or thick sheath (mode 3). The ram case assumes the cold ion current is best represented by a co-rotating flow [see (4)]. The thick sheath case, as described in [7], assumes the cold ions are best described by a Maxwellian plasma and a thick sheath (2). In reality, the actual current lies between these two limits but closer to the thick sheath limit (see discussion below).

Fig. 5 shows that even though the photoelectron flux is very low at Saturn (100 times lower than at the Earth), the plasma charging environment in sunlight is relatively benign. In shadow, surface potentials may reach a few tens to several hundred volts negative in the outer magnetosphere (the -128 V peak at 15.8 R_s is attributed to the assumption that the hot electron Kappa component dropped more abruptly in our environmental estimates than did the heavy ion co-rotating component in going from 16 to 18 R_s—perhaps due to the influence of Titan, outside 16 R_s the ion/electron ratio rises and suppresses the nominal charging levels).

However, this is not the worst case. The potentials were also estimated assuming that the spacecraft was in shadow and that either the cold heavy ions (as when they are shadowed on one side of the spacecraft) or the secondary electrons were suppressed. For the latter case (and either ram or thick sheath), the potential can reach over a thousand volts negative between 8

TABLE III
ESTIMATES OF THE CHARGING LEVELS AT SATURN AS A FUNCTION OF DISTANCE (R_s), CO-ROTATION VELOCITY (V_s), AND MODE (2 = RAM CURRENT FOR COLD IONS; 3 = THICK SHEATH ASSUMPTION FOR COLD IONS). FOUR CONDITIONS ARE LISTED: IN SUNLIGHT (SUN ON), IN SHADOW (SUN OFF), SUNLIGHT AND SECONDARY/BACKSCATTER EMISSION TURNED OFF (000), OR SUNLIGHT AND THE COLD HEAVY IONS TURNED OFF (I OFF). VALUES THAT ARE UNDERLINED AND IN BOLD ARE EXPECTED VALUES

Rs	Vs	Mode	Sun on	Sun off	000	I off
4.52	45	2	**10**	**10**	**-12**	-218
5.51	55	2	**10**	**10**	**10**	10
5.68	57	2	**-24**	**-32**	**-81**	-90
6.2	62	2	**1**	**0**	**-235**	**-53**
6.28	63	2	**10**	**10**	**10**	10
7.78	78	2	**0**	**-5**	**-1397**	-71
7.99	80	2	**0**	**-60**	-13125	-1231
8.75	88	2	**2**	**-30**	-62	-69
8.78	88	2	**0**	**-26**	(-)	-68
10.94	100	2	**0**	**-47**	-19688	-1504
11.59	100	2	**1**	**-24**	-7280	-47
14.96	100	2	**5**	**-10**	**-1581**	-43
15.14	100	2	**0**	-137	-8289	-1777
15.77	100	2	**0**	-649	-15142	-2256
18.05	100	2	**6**	**0**	**-1256**	**-6**
20.4	100	2	**8**	**0**	**-207**	**0**

Rs	Vs	Mode	Sun on	Sun off	000	I off
4.52		3	4	3	-34	**-35**
5.51		3	10	10	10	**5**
5.68		3	-32	-41	-73	**-62**
6.2		3	0	-8	-81	-33
6.28		3	10	10	10	**5**
7.78		3	0	-21	-235	**-47**
7.99		3	0	-47	**-743**	**-68**
8.75		3	2	-26	**-50**	**-42**
8.78		3	0	-27	**-496**	**-45**
10.94		3	0	-53	**-1211**	**-120**
11.59		3	1	-29	**-483**	**-39**
14.96		3	4	-16	-129	**-32**
15.14		3	0	**-81**	**-1119**	**-171**
15.77		3	0	**-128**	**-1354**	**-205**
18.05		3	5	0	-217	-3
20.4		3	8	0	-82	0

and 18 R_s. The assumption that the ion ram current dominates is strictly a worst case and not realistic as there is also a ion thermal "thick sheath" current present. In Table III, the most realistic of the worst case potentials for the model are indicated by bold letters and underlining. For the table, it is assumed that, whenever the thick sheath negative potential exceeds or is approximately equal to the equivalent ion or proton ram energy, the ions or protons will be attracted to the spacecraft as though the thick sheath applies. As an example, when at 18 R_s the ram estimate gives $-15\,000$ V for an estimate in shadow and for no secondaries, the thick sheath estimate is only -1100 V. The proton and ion ram "energies" are 53 eV and 840 eV. These values are less than the thick sheath potential and a great deal less than the ram estimate. This implies that the protons and ions will be isotropically attracted to the spacecraft overcoming the ram anisotropy—hence we assume the lower, thick sheath value is more appropriate for these conditions. Given this assumption, only for complete suppression of the secondary electron currents and photoelectron flux could the potential at Saturn ever exceed $\sim$1000 V—hopefully a rare occurrence.

Although Cassini was designed to be conductive on the outside to limit surface charging problems, this wasn't entirely successful. One of the authors was responsible for identifying areas on the vehicle where secondary emissions or the cold ion current could be suppressed. Indeed there may be such areas on Cassini but as all areas identified where charging or arcing may be a concern (e.g., near sensitive electronic circuitry) were covered with conducting materials before launch, surface charging-induced discharges will not likely impact the mission.

TABLE IV
ESTIMATES OF THE CHARGING LEVELS AS FUNCTIONS OF THE CONDITIONS LISTED IN TABLE III AND FOR THE MODE (2 = RAM CURRENT FOR COLD IONS; 3 = THICK SHEATH ASSUMPTION FOR COLD IONS). FOUR CONDITIONS ARE LISTED: IN SUNLIGHT (SUN ON), IN SHADOW (SUN OFF), SUNLIGHT AND SECONDARY/BACKSCATTER EMISSION TURNED OFF (000), OR SUNLIGHT AND THE COLD HEAVY IONS TURNED OFF (I OFF). VALUES THAT ARE UNDERLINED AND IN BOLD ARE EXPECTED VALUES. (NOTE: "(-)" MEANS THE VALUE IS INDETERMINATE AS MAY HAPPEN WHEN NOTHING CAN COMPENSATE FOR THE AMBIDNE ELECTRONS, E.G., GEOSYNCHRONOUS ORBIT WITH SECONDARY EMISSION AND SUNLIGHT TURNED OFF OUR MODEL HAS NO COMPENSATING CURRENT)

Region	Vs	Mode	Sun on	Sun off	000	I off
Earth						
Ionosphere	8	2	**-1**	**-1**	**-1**	(-)
Ionosphere		3	-1	-1	-1	(-)
Plasmasphere	8	2	**0**	**-1**	**-1**	(-)
Plasmasphere		3	0	-1	-1	(-)
Auroral Zone	8	2	**-1**	**-538**	**-8613**	(-)
Auroral Zone		3	-1	-1	-1	**-24541**
Geosynchronous	3	2	2	(-)	(-)	(-)
Geosynchronous		3	**2**	**-24541**	**-46963**	**-24541**
Jupiter						
Cold Torus	44	2	**-273**	**-820**	-37188	-1504
Cold Torus		3	-4	-24	**-459**	**-889**
Warm Torus	69	2	**-2**	**-2**	**-7315**	-3691
Warm Torus		3	-5	-6	-112	**-3145**
Hot Torus	85	2	**-20**	**-20**	**-128**	**-40**
Hot Torus		3	-28	-28	-102	-38
Plasmasheet	100	2	0	0	-1316	0
Plasmasheet		3	**0**	**0**	**-855**	**0**
Outer MgnSph	250	2	9	-4922	(-)	-4922
Outer MgnSph		3	**9**	**-889**	**-10203**	**-889**
Saturn						
Inner Plasmasheet	40	2	**0**	**-11**	-1128	**-43**
Inner Plasmasheet		3	0	-9	**-79**	-26
Extnd Pasmasheet	80	2	**0**	**-21**	-22832	**-60**
Extnd Pasmasheet		3	0	-25	**-602**	-41
Outer MgnSph	100	2	**2**	**0**	-4854	**-68**
Outer MgnSph		3	2	-6	**-584**	-34

V. DISCUSSION

Three examples (Figs. 2–5) of charging characteristics of the terrestrial, jovian, and saturnian environments have been provided. However, it is difficult from the potential maps to determine what the main components of the charging process were. In this section representative values of the environment for each of these planets (Table I) are compared so as to identify their primary differences. Each planet's environments are briefly discussed below.

For the Earth, the ionosphere, mid-plasmasphere, auroral zone, and geosynchronous orbit are described. The first three regions are dominated by the cold, dense ionospheric plasma. The auroral environment in addition occasionally experiences a similar high energy electron environment as that at geosynchronous orbit. For that environment, the worst case geosynchronous environment as presented in Purvis *et al.* [5] has been adopted. Table IV lists the corresponding potentials and, as in the case of Table III, the "best estimates" have been selected based on whether or not the thick sheath potential exceeded the equivalent ion ram energy. Table V presents the corresponding current terms in the absence of sunlight (tables

TABLE V

EQUILIBRIUM CURRENTS (PERCENTAGE) CORRESPONDING TO THE POTENTIALS IN TABLE IV FOR THE CASE OF NO SUNLIGHT. THE CURRENT TERMS ARE: c_{ec} = MAXWELLIAN ELECTRONS; c_{ek} = KAPPA ELECTRONS; c_{e2} = SECOND MAXWELLIAN ELECTRONS; c_h = COLD PROTONS; c_{hk} = KAPPA PROTONS; c_o = COLD IONS; c_{sep} = SECONDARIES DUE TO ELECTRONS; c_{bsp} = BACKSCATTERED ELECTRONS; c_{sip} = SECONDARIES DUE TO IONS. (NOTE: "(-)" MEANS INDETERMINATE)

Sun off		cec	cek	ce2	ch	chk	co	csep	cbsp	csip
Earth	**Mode**									
Ionosphere	2	100	0	0	0	0	77	1	22	0
Ionosphere	3	100	0	0	0	0	77	1	22	0
Plasmasphere	2	100	0	0	0	0	77	1	22	0
Plasmasphere	3	100	0	0	0	0	77	1	22	0
Auroral Zone	2	0	0	100	0	0	51	16	22	10
Auroral Zone	3	18	0	82	1	0	61	13	22	3
Geosynchronous	2	(-)	(-)	(-)	(-)	(-)	(-)	(-)	(-)	(-)
Geosynchronous	3	0	0	100	11	0	0	16	22	51
Jupiter										
Cold Torus	2	0	100	0	0	4	2	69	22	3
Cold Torus	3	0	100	0	0	3	4	69	22	2
Warm Torus	2	22	78	0	0	1	16	55	22	6
Warm Torus	3	0	100	0	0	1	7	69	22	1
Hot Torus	2	71	29	0	0	5	21	37	22	14
Hot Torus	3	51	49	0	0	9	18	49	22	3
Plasmasheet	2	54	46	0	0	19	1	30	50	0
Plasmasheet	3	54	46	0	0	19	0	31	50	0
Outer MgnSph	2	0	100	0	3	0	0	69	22	6
Outer MgnSph	3	0	100	0	4	0	0	69	22	5
Saturn										
Inner Plasmasheet	2	51	49	0	2	0	17	59	22	0
Inner Plasmasheet	3	53	47	0	4	0	15	58	22	0
Extnd Pasmasheet	2	29	71	0	1	0	5	69	22	2
Extnd Pasmasheet	3	27	73	0	3	0	4	70	22	0
Outer MgnSph	2	35	65	0	2	0	4	71	22	1
Outer MgnSph	3	32	68	0	2	0	4	71	22	1

for currents for all the cases are available but only the "sun off" case is presented for the sake of brevity). As would be expected, for the ionosphere and plasmasphere, 100% of the electron current is due to the ambient ionospheric electrons. What is of interest, however, is that although 77% of the positive current to the spacecraft is from the co-rotating ions, 22% is from the backscattered electrons. This is because the cold plasma generates few if any secondary particles.

For the auroral region, either all or most of the current is due to the higher energy electron component. Thus, the secondary terms become more important with the cold ion current dropping somewhat. A similar situation is found at geosynchronous where the secondary electrons emitted by ion impact are by far the major component—the ambient ion current only contributing about 11%. (Note: in Table V as the proton ram component is ~0, the ram case leads to unrealistic results in the Earth's environment since the radiation environment above 100 keV and the secondary currents from aluminum are insufficient to balance the incident electron currents—on the other hand, many materials do have sufficiently high secondary and backscatter components so that charging can be suppressed in these conditions—Indium Tin Oxide coating be a case in point. These points are noted by a "(-).")

For Jupiter, representative values for the cold electrons, cold protons and ions (thick sheath and co-rotating), and the hot electrons and protons (Kappa distributions) have been applied. Five characteristic regions between 3.5 and 20 R_j are assumed. These are the cold torus (3.5 to 5.5 R_j), the warm torus (5.5 to 7 R_j), the plasmasheet (8–20 R_j), and the outer magnetosphere (>20 R_j). The main difference between the torus regions is that

TABLE A1

TWO MAXWELLIAN PLASMA DISTRIBUTION FITS TO THE ELECTRON LOW ENERGY PLASMA ($E < 10$ keV) DATA FROM VOYAGER 1 (V1) AND VOYAGER 2 (V2) FLYBYS OF SATURN. THE VARIABLES ARE: L—THE L-SHELL OF THE OBSERVATION; R_{E1}—LOW ENERGY PLASMA DENSITY (cm^{-3}); T_{E1}—LOW ENERGY PLASMA TEMPERATURE (eV); R_{E2}—WARM PLASMA DENSITY (cm^{-3}); T_{E2}—WARM PLASMA TEMPERATURE (eV)

ELECTRON DISTRIBUTIONS FOR E<10 keV					
SAT	L	RE1	TE1	RE2	TE2
V1	20.4	3.49E-02	46.03	8.86E-03	300.17
V1	15.0	1.65E-01	27.42	1.47E-02	550.77
V1	10.9	4.49E-01	25.79	3.26E-02	532.76
V1	8.8	9.46E-01	26.25	1.01E-01	568.74
V1	6.3	---	---	3.73E-02	20.00
V1	5.5	5.61E-02	16.10	2.83E-03	150.53
V1	5.7	1.02E+01	23.17	2.53E-01	584.97
V1	8.8	7.79E-01	32.68	7.19E-02	582.17
V2	15.8	1.53E-01	37.55	2.21E-02	435.76
V2	11.6	4.58E-01	22.95	4.82E-02	342.13
V2	7.8	1.41E+00	26.48	1.00E-01	418.05
V2	4.5	---	---	9.81E-02	11.45
V2	6.2	1.24E+00	22.37	6.16E-02	387.31
V2	8.0	9.47E-01	33.94	1.52E-01	468.14
V2	15.1	1.16E-01	47.31	1.91E-02	436.88
V2	18.1	4.04E-02	46.93	5.34E-03	255.66

the density and temperature of the electrons and ions rise as radial distance increases. Likewise, the co-rotation velocity rises. As illustrated in Fig. 3 and Table IV, an inner region of high charging is predicted inside the orbit of Io. In the model (see Table V), the primary source of this region, if it exists, is the hot (Kappa) electron population which balances mainly with its secondaries. At radial distances greater than Io's orbit (5.9 R_j), the cold heavy ion population increases dramatically. It is suspected that the inner charging region corresponds somewhat to the plasmapause/geosynchronous orbit boundary at Earth and, if it were not for the Io torus beginning at 5.9 R_j, charging would increase steadily as R_j increased. Indeed, the potentials inside Io are similar to those in the outer magnetosphere where there is no heavy ion component. Current balance (Table V) is very similar for the cold torus and the outer magnetosphere—69% secondary electrons and 22% backscattered electrons. Suppressing the secondary electrons forces charge balance with the proton Kappa component and the heavy ions in the inner magnetosphere, hence the high potentials. In the outer magnetosphere of Jupiter, as at the Earth, in the absence of sunlight and secondaries, the hot electrons balance with the hot protons giving high potentials.

For the representative saturnian environments in Table II, the 16 spectra were averaged over three regions: inner plasmasheet (4–8 R_s), extended plasmasheet (8–12 R_s), and outer magnetosphere (12–20 R_s). The resulting potentials are similar to those in Fig. 5 if not slightly lower as they are the results of average environments. Setting the photoelectron flux to 0 has little effect on the potential even between 12–20 R_s, probably because the photoelectron flux is already 1/100 what it is at the Earth. The biggest effect appears to be turning off the secondary electrons as this forces the hot electrons (Kappa) in the extended plasmasheet and outer magnetosphere to balance with the cold protons and ions (in reviewing the current balance for this case,

TABLE A2
KAPPA PLASMA DISTRIBUTION FITS TO THE ELECTRON HIGH ENERGY PLASMA DATA FROM VOYAGER 1 (V1) AND VOYAGER 2 (V2) FLYBYS OF SATURN. THE VARIABLES ARE: L—THE L-SHELL OF THE OBSERVATION; R_{EK}—KAPPA ELECTRON DENSITY (cm^{-3}); T_{EK}—KAPPA ELECTRON TEMPERATURE (eV); K_E—ELECTRON KAPPA CONSTANT

ELECTRON KAPPA DISTRIBUTIONS				
SAT	L	REK	TEK	KE
V1	20.4	8.17E-03	252.04	2.41
V1	15.0	8.28E-03	306.58	1.57
V1	10.9	7.52E-02	808.43	2.11
V1	8.8	5.29E-03	48.00	0.84
V1	6.3	2.28E-02	10.64	1.17
V1	5.5	1.49E-02	373.59	1.61
V1	5.7	5.60E-02	164.77	1.29
V1	8.8	6.20E-02	413.85	1.37
V2	15.8	8.63E-02	976.78	2.82
V2	11.6	4.38E-02	268.55	1.74
V2	7.8	1.49E-01	482.72	2.45
V2	4.5	8.24E-01	41.31	2.17
V2	6.2	1.09E-01	498.33	2.25
V2	8.0	3.68E-01	749.28	2.45
V2	15.1	6.74E-02	932.80	3.35
V2	18.1	1.43E-02	449.09	2.96

TABLE A3
KAPPA PLASMA DISTRIBUTION FITS TO THE PROTON HIGH ENERGY PLASMA DATA FROM VOYAGER 1 (V1) AND VOYAGER 2 (V2) FLYBYS OF SATURN. THE VARIABLES ARE: L—THE L-SHELL OF THE OBSERVATION; R_{HK}—KAPPA PROTON DENSITY (cm^{-3}); T_{HK}—KAPPA PROTON TEMPERATURE (eV); K_E—PROTON KAPPA CONSTANT

SAT	L	RHK	THK	KH
V1	20.4	1.70E-03	16000	7.0
V1	15.0	3.00E-03	13000	5.7
V1	10.9	3.00E-03	21000	6.3
V1	8.8	5.00E-03	25000	6.3
V1	6.3	1.00E-02	23000	7.0
V1	5.5	1.00E-02	23000	7.0
V1	5.7	2.30E-03	28000	7.7
V1	8.8	2.30E-03	28000	7.7
V2	15.8	1.60E-03	30000	7.3
V2	11.6	1.30E-03	45000	15.0
V2	7.8	2.70E-03	35000	8.0
V2	4.5	3.30E-03	35000	7.4
V2	6.2	3.30E-03	35000	7.4
V2	8.0	3.30E-03	35000	7.4
V2	15.1	3.00E-04	20000	7.0
V2	18.1	1.50E-04	15000	6.5

TABLE A4
MAXWELLIAN PLASMA DISTRIBUTION FITS TO THE PROTON LOW ENERGY PLASMA DATA FROM VOYAGER 1 (V1) AND VOYAGER 2 (V2) FLYBYS OF SATURN. THE VARIABLES ARE: L—THE L-SHELL OF THE OBSERVATION; R_{HC}—COLD PROTON DENSITY (cm^{-3}); T_{HC}—COLD PROTON PLASMA TEMPERATURE (eV); V_{ROT}—ASSUMED CO-ROTATION VELOCITY (Km/s)

SAT	L	RHC	THC	VROT
V1	20.4	0.250	50	100
V1	15.0	0.250	30	100
V1	10.9	0.250	30	100
V1	8.8	1.000	25	88
V1	6.3	2.200	10	63
V1	5.5	8.830	12	55
V1	5.7	2.250	12	57
V1	8.8	0.679	20	88
V2	15.8	0.250	30	100
V2	11.6	0.290	40	100
V2	7.8	1.100	25	78
V2	4.5	3.160	10	45
V2	6.2	1.640	15	62
V2	8.0	1.500	17	80
V2	15.1	0.218	35	100
V2	18.1	0.218	40	100

TABLE A5
MAXWELLIAN PLASMA DISTRIBUTION FITS TO THE OXYGEN ION LOW ENERGY PLASMA DATA FROM VOYAGER 1 (V1) AND VOYAGER 2 (V2) FLYBYS OF SATURN. THE VARIABLES ARE: L—THE L-SHELL OF THE OBSERVATION; R_{HC}—COLD OXYGEN ION DENSITY (cm^{-3}); T_{OC}—COLD OXYGEN ION PLASMA TEMPERATURE (eV); V_{ROT}—ASSUMED CO-ROTATION VELOCITY (Km/s)

SAT	L	ROC	TOC	VROT
V1	20.4	0.550	450	100
V1	15.0	0.550	425	100
V1	10.9	1.000	380	100
V1	8.8	3.600	200	88
V1	6.3	30.000	60	63
V1	5.5	29.200	40	55
V1	5.7	27.500	80	57
V1	8.8	2.660	250	88
V2	15.8	0.500	400	100
V2	11.6	0.750	300	100
V2	7.8	11.300	100	78
V2	4.5	59.000	80	45
V2	6.2	23.900	80	62
V2	8.0	4.510	100	80
V2	15.1	0.600	400	100
V2	18.1	0.500	425	100

it appears that the cold ions dominate for the ram case and the cold protons for the thick sheath). Apparently the overall lower densities/temperatures of the hot electron (Kappa) component at Saturn compared to Jupiter (Table II) is responsible for the somewhat lower voltages estimated at Saturn.

VI. CONCLUSION

A simple design tool based on current balance and on the Earth's, Jupiter's, and Saturn's plasma environments has been used to estimate the spacecraft-to-space potentials for missions to these planets. The results of this tool, a predicted range of worst case surface potentials, for a spherical spacecraft with aluminum surfaces are presented in Table IV for the Earth, Jupiter, and Saturn. Based on this table, the Earth clearly represents the worst threat to spacecraft. Negative potentials as high as 25 000 V are predicted near geosynchronous orbit in eclipse and, indeed, potentials in excess of −20 000 V have apparently been observed. At Jupiter, potentials are more moderate, −900 V in the outer magnetosphere being the largest predicted for eclipse conditions. Large potentials are only observed if, in addition to being in shadow, secondary emissions or the co-rotating ions can be suppressed–unlikely but possible for some surface configurations. Conditions at Saturn are similar to those at Jupiter, though charging is lower in general. Even so, spacecraft surface

charging is still a concern for spacecraft survivability at these planets as differential potentials of ~100 V are believed to be capable of causing surface arcing in some cases. Indeed, as potentials of even a few tens of volts can seriously affect low energy plasma measurements, spacecraft charging must be carefully considered for scientific missions to these planets.

APPENDIX

The following Tables A1-A5 list the input plasma parameters used in estimating the saturnian charging environment. They are derived from Voyager plasma and energetic particle data as outlined in the text.

ACKNOWLEDGMENT

Special thanks go to Dr. A. R. Frederickson and A. C. Whittlesey who both carefully and patiently reviewed the text.

REFERENCES

[1] S. E. DeForest and C. E. McIlwain, "Plasma clouds in the magnetosphere," *J. Geophys. Res.*, vol. 76, p. 3587, 1971.
[2] M. S. Gussenhoven, "High level spacecraft charging in the low altitude polar auroral environment," *J. Geophys. Res.*, vol. 90, pp. 11 009–11 023, 1985.
[3] C. K. Purvis, "Jupiter probe charging study," NASA TP-1263, NASA Lewis Res. Center, 1979.
[4] T. N. Divine and H. B. Garrett, "Charged particle distributions in Jupiter's magnetosphere," *J. Geophys. Res.*, vol. 88, no. A9, pp. 6889–6903, Sept. 1983.
[5] C. K. Purvis, H. B. Garrett, A. C. Whittlesey, and N. J. Stevens, "Design guidelines for assessing and controlling spacecraft charging effects," NASA TP-2361, NASA, 1984.
[6] P. Tsipouras and H. B. Garrett, "Spacecraft charging model, 2 Maxwellian approximation," AFGL-TR-79-0153, AFGL, 1979.
[7] H. B. Garrett, "The charging of spacecraft surfaces," *Rev. Geophys.*, vol. 19, pp. 577–616, 1981.
[8] J. D. Richardson and E. C. Sitler, Jr., "A plasma density model for Saturn based on Voyager observations," *J. Geophys. Res.*, vol. 95, pp. 12 019–12 031, 1990.
[9] V. M. Vasyliunas, "A survey of low-energy electrons in the evening sector of the magneteosphere with OGO 1 and OGO 3," *J. Geophys. Res.*, vol. 73, p. 2839, 1968.
[10] R. Evans, H. B. Garrett, S. Gabriel, and A. C. Whittlesey, "A preliminary spacecraft charging map for the near earth environment," in *Proc. Spacecraft Charging Technol. Conf.*, 1989.
[11] R. L. McNutt, Jr., "The dynamics of the low energy plasma in the Jovian magnetosphere," dissertation, Massachusetts Institute of Technology, Cambridge, MA, 1980.
[12] J. D. Scudder, E. C. Sittler, Jr., and H. S. Bridge, "A survey of the plasma electron environment of Jupiter: A view from Voyager," *J. Geophys. Res.*, vol. 86, pp. 8157–8179, 1981.
[13] K. K. Khurana, M. G. Kivelson, T. P. Armstrong, and R. J. Walker, "Voids in Jovian magnetosphere revisted: Evidence of spacecraft charging," *J. Geophys. Res.*, vol. 92, no. A12, pp. 13 399–13 408, 1987.
[14] P. Leung, A. C. Whittlesey, H. B. Garrett, P. A. Robinson, Jr., and T. N. Divine, "Environment-induced electrostatic discharges as the cause of Voyager 1 power-on resets," *J. Spacecraft*, vol. 23, no. 3, pp. 323–330, May/June 1986.
[15] I. Katz, D. E. Parks, M. J. Mandell, J. M. Harvey, S. S. Wang, and J. C. Roche, "NASCAP, a three-dimensional charging analyzer program for complex spacecraft," *IEEE Trans. Nucl. Sci.*, vol. NS-24, p. 2276, 1977.
[16] I. Katz, J. J. Cassidy, M. J. Mandell, G. W. Schnuelle, P. G. Steen, and J. C. Roche, "The capabilities of the NASA charging analyzer program," *Spacecraft Charging Technol.*, 1978. NASA, NASA CP-2071/AFGL-TR-79-0082.
[17] S. M. Krimigis and J. F. Carbary *et al.*, "General characteristics of hot plasma and energetic particles in the Saturnian magnetosphere: Results from the Voyager spacecraft," *J. Geophys. Res.*, vol. 88, pp. 8871–8892, 1983.
[18] S. Maurice and E. C. Sitler, Jr. *et al.*, "Comprehensive analysis of electron observations at Saturn: Voyager 1 and 2," *J. Geophys. Res.*, vol. 101, pp. 15 211–15 232, 1996.

Henry B. Garrett was born on February 15, 1948 in San Francisco, CA. He was raised in Roswell, NM, graduating from Roswell Senior High School in 1966. He received the B.A. degree in physics (Phi Beta Kappa, magna cum laude) in 1970 and the M.S. and Ph.D. degrees in space physics and astronomy from Rice University in 1974. He subsequently spent 6 years in the US Air Force before joining the Jet Propulsion Laboratory, California Institute of Technology in 1980. He is currently the Lead Technologist, Safety and Mission Assurance Directorate. He is a member of AIAA, AGU, and AAS and a Colonel in the USAF Reserves assigned to the Space and Missile Center, CA.

Alan R. Hoffman was born in Ft. Morgan, Colorado, on August 23, 1940. He received the B.A. degree in physics from Colorado University, Boulder, Colorado in 1962. He received the M.S. degree in mathematics from the University of Southern California, Los Angeles, CA in 1967. He joined the Jet Propulsion Laboratory, California Institute of Technology, Pasadena, CA in 1962 and is currently a Principal, Member of the Technical Staff in the Office of Reliability Engineering. He is engaged in efforts and research related to planning and implementing environmental test and analysis programs for unmanned planetary spacecraft. He has received NASA Exceptional Service Medals for his contributions to Galileo and Cassini and NASA Group Achievement Awards for Ranger VII, Mariner 9, Viking, Voyager, Galileo, Cassini, and Deep Space 1 flight projects.